VERSITA

Acta Geophysica
vol. 62, no. 6, Dec. 2014, pp. 1283-1309
DOI: 10.2478/s11600-013-0194-1

A Detailed Analysis of Microseismicity in Samos and Kusadasi (Eastern Aegean Sea) Areas

Onur TAN[1], Eleftheria E. PAPADIMITRIOU[2], Zumer PABUCÇU[1], Vassilis KARAKOSTAS[2], Ahmet YÖRÜK[1], and Kostas LEPTOKAROPOULOS[2]

[1]TÜBİTAK Marmara Research Center, Earth and Marine Sciences Institute, Gebze, Turkey

[2]Geophysics Department, School of Geology, Aristotle University of Thessaloniki, Thessaloniki, Greece; e-mail: ritsa@geo.auth.gr

Abstract

A detailed investigation of microseismicity and fault plane solutions are used to determine the current tectonic activity of the prominent zone of seismicity near Samos Island and Kusadasi Bay. The activation of fault populations in this complex strike-slip and normal faulting system was investigated by using several thousand accurate earthquake locations obtained by applying a double-difference location method and waveform cross-correlation, appropriate for areas with relatively small seismogenic structures. The fault plane solutions, determined by both moment tensor waveform inversions and *P*-wave first motion polarities, reveal a clear NS trending extension direction, for strike slip, oblique normal and normal faults. The geometry of each segment is quite simple and indicates planar dislocations gently dipping with an average dip of 40-45°, maintaining a constant dip through the entire seismogenic layer, down to 15 km depth.

Key words: microearthquake activity, seismotectonics, transtension, eastern Aegean.

1. INTRODUCTION

In 31 July 2007 online seismological stations were deployed in the central part of the Aegean coast of western Turkey (Inan *et al.* 2007, Tan 2013). Since then, continuous monitoring of microseismicity was made, resulting in a wealth of data which, along with data provided from seismological stations of the permanent Hellenic Unified Seismological Network (HUSN), are capable to reveal the geometry and kinematic properties of the activated structures. Here we present a detailed look at the seismicity of the Samos and Kusadasi area, between 37.5-38.0° and 26.5-27.5°, as recorded by the local network for a period of more than 5 years (July 2007 – September 2012). There have been a number of detailed studies of neotectonic analysis of the study area (*e.g.*, Bozkurt 2001, 2003, Genç *et al.* 2001, Gurer *et al.* 2001, Çiftçi and Bozkurt 2009), seismological studies focused on the fault population of the area (Aktar *et al.* 2007), and seismic prospecting (Kurt *et al.* 1999, Ocakoğlu *et al.* 2004). The above studies provide a background upon which we may discuss our findings.

The study area occupies the central eastern part of the Aegean microplate, a highly deformed extensional back-arc area. The subduction of the eastern Mediterranean oceanic plate under the Aegean microplate (Papazachos and Comninakis 1971) and the westwards motion of the Anatolian microplate along the North Anatolian Fault (McKenzie 1972, 1978) condition the regional deformation pattern (Fig. 1). The velocity field, expressed in a Eurasia fixed reference frame in the eastern Mediterranean area is dominated by a general counter-clockwise rotation, with increasing magnitude of velocity towards the Hellenic trench. The motion of the Anatolian microplate is transferred in the Aegean area as a simple translation, taking place along the central and southern part of the Turkish coastal area and the neighboring Greek Islands. The Aegean area moves almost uniformly in a SSW direction (~ 200-220°) with an average velocity of ~30 mm/yr, which increases from 25 mm/yr in the central and southern part of the western coast of Turkey to 30-35 mm/yr near the south western part of the Hellenic Arc (Papazachos 1999), with a significant increase being due to the strong N-S extension in the Aegean and western Turkey (McClusky *et al.* 2000). West of the longitude of 31°E, Anatolia undergoes predominantly NS stretching, leading to up to 30 mm/yr total extension from the Sea of Marmara and to Mediterranean coast (Aktug *et al.* 2009).

As a result of the above motions, the northern Aegean area is dominated by dextral strike-slip faulting of northeasterly strike, with their conjugate left-lateral ones, which are nearly orthogonal to the main right-lateral faults that they abut, co-existing with normal faulting (Taymaz *et al.* 1991, Papazachos *et al.* 1998, Karakostas *et al.* 2003). The back arc extension is

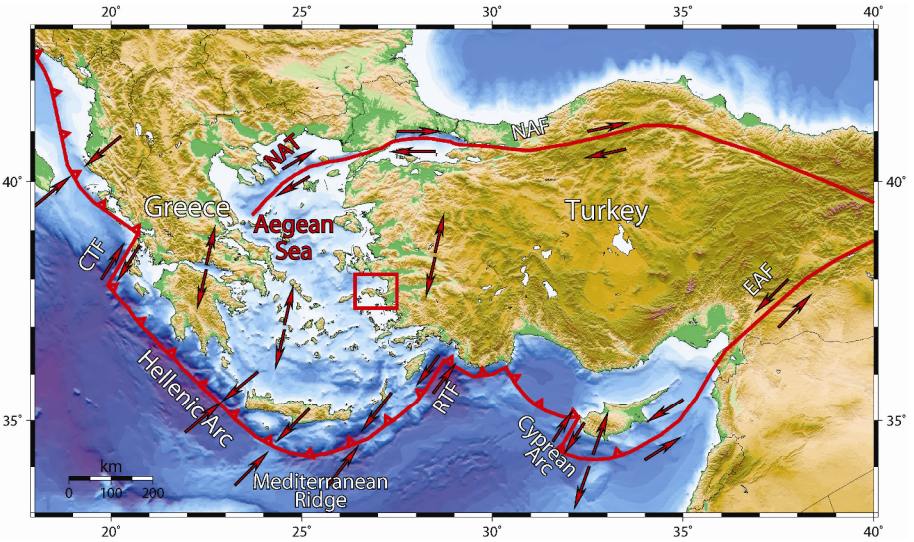

Fig. 1. Eastern Mediterranean region with the major active boundaries and the sense of relative motions. The study area is denoted by the rectangle. CTF – Cephalonia Transform Fault, NAT – North Aegean Trough, NAF – North Anatolian Fault, EAF – East Anatolian Fault. Colour version of this figure is available in electronic edition only.

present in the Aegean and the western coastal area of Turkey, where it produced broad and complex systems of normal faults, usually bounding the extensional basins that are characteristically placed in parallel, with current rate of extension equal to 6 mm/yr (McClusky *et al.* 2000, Nocquet 2012). The transition zone between dextral strike slip and normal faulting of central East Aegean comprises a set of oblique faults that are comprised in our study area.

Previous studies focused in seismotectonic properties of the study area concerned either mapping of active faults (*e.g.*, Mountrakis *et al.* 2003), study of seismic sequences (*e.g.*, Benetatos *et al.* 2006) or microseismicity analysis (*e.g.*, Tan 2013). The aim of this study is to illuminate the subsurface structure of the mapped faults using hypocenter locations of crustal seismicity registered with a dense local network. This approach is appropriate since the location errors are much smaller than the dimensions of the faults that have to be studied and the smaller ones identified here. Here we analyze the seismicity and identify faults that appear related to certain clusters. The abundant event number comprised in each cluster, along with location accuracy, helps to identify the architecture of the fault population and clarify fault geometry. We extend our efforts and present new seismological evidence for microseismicity associated with active regional normal faults

located in Samos Island and in Kusadasi area. The results are compared with recent regionally recorded seismic activity and with previous micro-seismicity studies near the study area.

2. REGIONAL SEISMICITY AND TECTONIC SETTING

The area of eastern Aegean along with the western coasts of Turkey consist a part of a transition zone of deformation, with a width of the order of 100 km, where the change from the Anatolian movement is translated to the Aegean (Papazachos 1999). The Aegean Sea is characterized by dextral strike-slip faulting along NE-SW striking faults, along fault zones formed parallel to the North Aegean Trough (NAT). The strongest (up to 7.4) earthquakes during the instrumental era are associated with this kind of faulting, whereas their conjugate sinistral strike-slip counterparts are also active (*e.g.*, the 26 July 2001 Skyros $M = 6.3$ main shock, Karakostas *et al.* 2003). Less frequent but not absent are the strong events associated with predominantly normal faulting, like the 1967 $M = 6.7$ earthquake (McKenzie 1972). Pure strike slip faulting is changing to oblique, with significant component of extension, as one goes from the Aegean to the coastal area of western Turkey. The onshore deformation in western Turkey is dominated by crustal extension and confirmed by rather frequent earthquakes along grabens, the formation of which is attributed either to the N-S extensional regime and subsequently they are coeval, or they are produced by successive events and have been formed under different tectonic regimes (Genç *et al.* 2001). Nevertheless, strike slip faulting is also present, which onshore results in oblique normal faults and becomes more evident in the Karaburun peninsula and offshore area. The strike-slip faulting, that has previously been thought only to accommodate variations in extension between adjacent normal faults, is now suggested to be of greater importance because there is considerable evidence of zones of deformation, some of which may be linked to the strike-slip faulting onshore (Ocakoğlu *et al.* 2004).

The study area has been repeatedly visited by strong ($M \geq 6.0$) events as both historical record and instrumental data reveal (stars in Fig. 2). Although spatial clusters are formed, this is evidently due to the macroseismic observations that are related with the significant historical cities prospered there since the classical antiquity (a few centuries BC). Nevertheless, it is also evident that Samos Island has repeatedly been visited by earthquakes that have produced extensive damage and for this reason their macroseismic epicenter was evaluated onshore or offshore the island (Table 1). The frequent visit of strong earthquakes predicates knowledge on the geometry and kinematics of the faults that are possibly associated with these strong events, and in particular the onshore ones, constituting a major threat since they are close or pass through inhabited areas. It became then evident the importance of the accu-

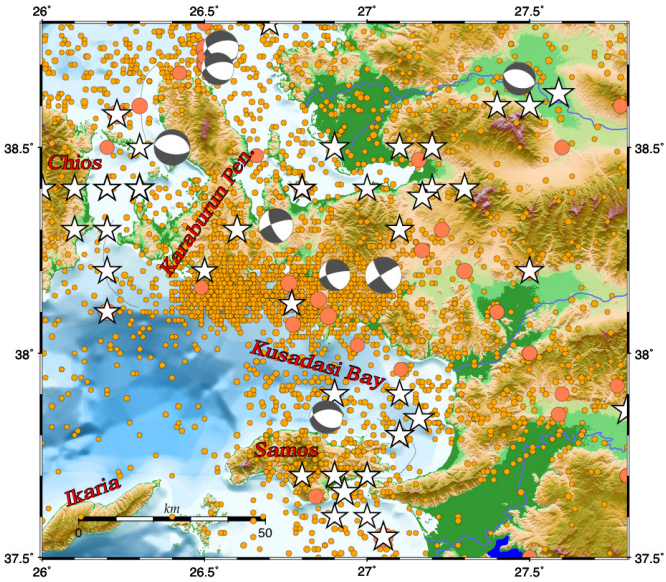

Fig. 2. Spatial distribution of regional seismicity in the central-eastern Aegean area (more than 13 500 events between July 2007 and September 2012). Stars denote epicenters of the known historical earthquakes with $M > 6.0$, whereas larger and smaller circles earthquakes of $M > 5.0$ and $M > 3.5$, that occurred in the study area since 1911 and 1981, respectively. The available fault plane solutions from GCMT routine analysis are shown as lower-hemisphere equal-area projections. Colour version of this figure is available in electronic edition only.

Table 1

Strong ($M > 6.0$) historical earthquakes reported for Samos Island and the adjacent Turkish coastal area

Date	Location		M	Place and maximum intensity
	Latitude (°N)	Longitude (°E)		
200 BC	37.70	26.90	6.3	Samos (VIII)
47 AD	37.84	27.16	6.9	Samos (VIII)
18 Jun 1751	37.80	27.10	6.9	Samos (VIII)
3 Apr 1831	37.70	26.80	6.0	Samos (VII)
13 Jun 1846	37.60	27.00	6.0	Samos (VII)
11 Oct 1865	37.70	27.00	6.0	Samos (VII)
3 May 1868	37.60	26.90	6.0	Samos (VII)
31 Jan 1873	37.80	27.10	6.5	Samos (VII)
14 Oct 1877	37.70	27.00	6.0	Samos (VIII)
14 Dec 1890	37.90	27.10	6.2	Ephesus (VIII)
12 Mar 1893	37.90	26.90	6.6	Samos (VII)
11 Aug 1904	37.66	26.93	6.8	Samos (VIII)
16 Jul 1955	37.55	27.05	6.9	B. Menderes (VIII)

rately located microseismicity employment for the identification of these faulting properties that will provide precious input for the regional seismic hazard assessment.

3. LOCAL NETWORK AND MICROSEISMICITY LOCATION

In order to investigate the geometry of the fault network in the study area, microseismicity was exploited from the recordings of a local network installed in the framework of TURDEP Project (Inan *et al.* 2007) and operated during July 2007 – December 2012. Maintenance of the network and data collection and analysis were then performed for the scope of the current research bilateral project between Greece and Turkey (Tan 2013). Azimuthal coverage was improved by incorporating data from the permanent Hellenic National Seismological Network. The seismological stations are equipped with broadband seismometers (Güralp 40T, 3TD, ESP3; Trillium 120P) and 100 sps high resolution recorders (Güralp DM24, Reftek 130). The online data acquisition from the stations is carried out via direct internet lines or GPRS modems. The daily manual phase readings of the events were implemented carefully, and catalog contamination from quarry blasts is prevented. In total, 32 458 *P*- and 21 865 *S*-arrivals were used for the earthquake location, contributed to a considerably accurate focal parameters determination. Tan (2013) has checked and showed through an hourly event histogram that the catalog does not contain major seismic activity during the daytime hours. To the contrary, when he investigated the seismic activity above the threshold magnitude into two separate data sets, the one being during the daytime and the second in nighttime, he found out that the first was smaller than the latter, but without any significant difference.

Earthquake location was achieved using the hypocenter location algorithm described by Lienert and Havskov (1995). A multilayered *P*-velocity model derived from seismic tomography is used (Akyol *et al.* 2006, Table 2) for locating more than 13 500 events in the region shown in Fig. 2. In our study area, comprising Samos Island and Kusadasi, about 4610 events occurred with $M_L > 0.3$, with mean horizontal and vertical location uncertainties equal to +3.3 and +4.6 km, respectively, and a mean RMS value of about 0.2 s (Fig. 3). The largest uncertainty in depth calculation is partly due to the fact that the closest station is at a distance of at least twice the depth value. In general, one additional reason for location uncertainties is due to the fact that the western part of the study area is submarine and therefore the azimuthal gaps are high for most of the events, with an average value of 170°.

Relocation was afterwards performed by the use of a double-difference inversion algorithm (hypoDD) developed by Waldhauser and Ellsworth (2000), the description of which is widely and often published, and for this

Table 2

P-wave velocity (V_p) model
used for the earthquake locations
(Akyol *et al*. 2006)

Depth [km]	V_p [km/s]
0.0 – 1.5	4.7
1.5 – 3.0	5.1
3.0 – 5.0	5.8
5.0 – 15.0	6.0
15.0 – 21.0	6.3
21.0 – 29.0	6.4
29.0 – ∞	7.8

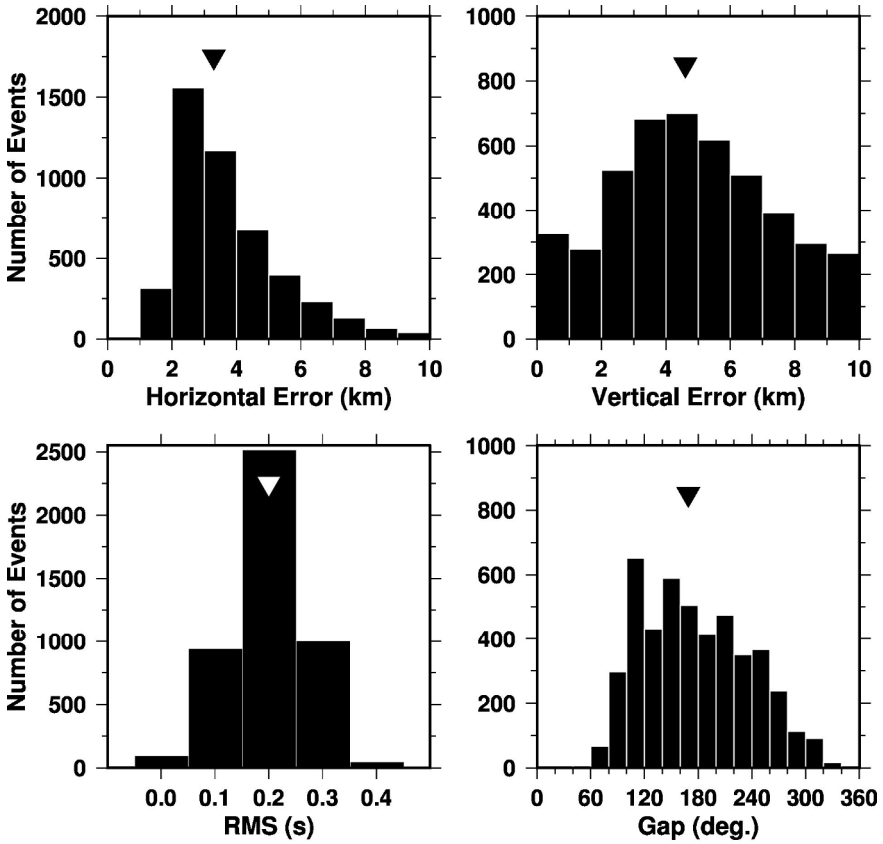

Fig. 3. Histograms showing location uncertainties for about 4610 events, with mean values depicted by inverted triangles.

reason is not repeated here. The absolute location parameters from the first catalog were used as the initial input of the relocation inversion procedure. The *P*/*S* travel time differences between the event pairs were the input data and additionally, the high-precision differential travel times from the phase correlation of *P*- and/or *S*-wave (cross-correlation, CC) data were used. The differential travel-time data, with a relative timing precision of approximately tens of ms, allows for the calculation of the relative location between earthquakes with errors of only a few hundreds of meters. The location uncertainties of the large data set can be estimated using statistical resampling methods (Waldhauser and Ellsworth 2000). Here the statistical approach described in Tan *et al.* (2010) was used. More than a million event locations were obtained to include in the statistical distribution. The outliers in the dataset were removed using the interquartile range (IQR) method. More than 90% of the total samples remained after the IQR analysis. The horizontal and vertical location errors were calculated as ± 1000 and ± 2000 m, respectively.

Local magnitudes were determined as described in Tan (2013), with the lower M_L magnitude limit of the data set being approximately 0.3. Magnitudes range between 0.5 and 5.1 (the main shock of the 20 June 2009, Samos sequence) and the completeness of the catalogue is $M_c = 1.4$, with a *b*-value equal to 0.9, close to unit, which characterizes regular background seismicity (Fig. 4). The small completeness magnitude verifies that this catalogue is the best data set for the study area.

Seismicity spatial distribution (Fig. 5) reveals certain clusters, the most prominent of them being in the offshore Cesme area, Karaburun Peninsula, Izmir Gulf, onshore and offshore of Kusadasi and onshore and offshore Samos Island. The latter clusters, in Kusadasi and Samos area, will be investi-

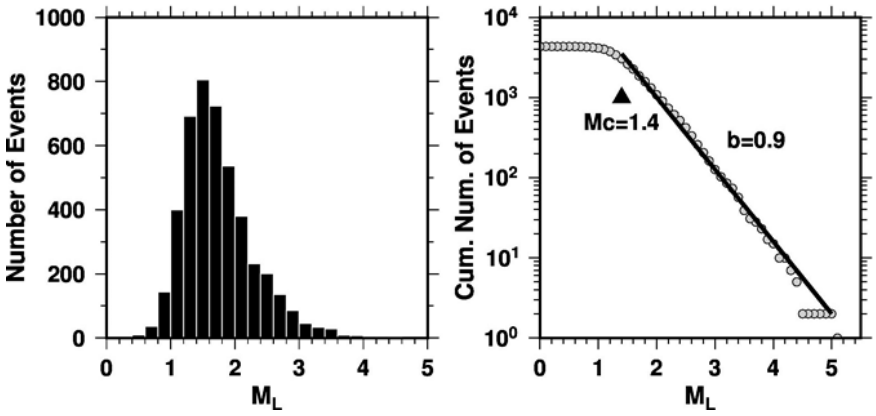

Fig. 4. Cumulative number of earthquakes *versus* magnitude (completeness magnitude, $M_c = 1.4$).

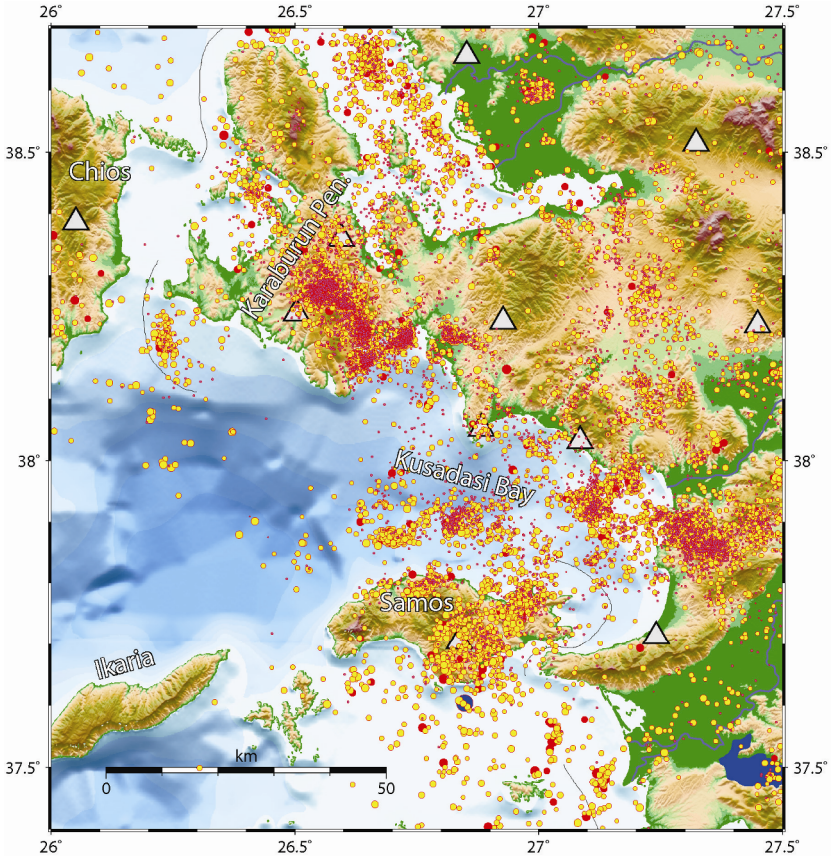

Fig. 5. Spatial distribution of local microseismicity monitored for about 5 years (2007-2012). Triangles denote the positions of local temporary seismological stations in western Turkey, and permanent ones onto the Islands of Chios and Samos, belonging to the National Hellenic Unified Seismological Network. Colour version of this figure is available in electronic edition only.

gated in detail in the following section, since they are comprised inside our study area and constitute our tools to unravel geometry and kinematic properties of the associated faults.

4. FAULT PLANE SOLUTIONS

Focal mechanisms were determined for 19 earthquakes, ranging in magnitudes between 3.6 and 5.1, for which adequate information became available, either by using the polarities of the *P*-wave first motions (FMP) using the "focmec" algorithm (Snoke *et al.* 1984), or waveform inversion with the ISOLA (Sokos and Zahradnik 2008) regional local moment tensor (RMT) inversion algorithm (Table 3, Appendices A and B). The keen interest for

Table 3

Information on source parameters for 19 events, and 3 joint solutions (with 5, 9, 14 events, respectively) that occurred in the study area during 2008-2012

	Date	Origin time h:m	Epicentral coordinates		h [km]	H [km]	M_L	M_w	M_0 [$\times 10^{14}$ Nm]	Fault plane			FPS type
			Lat. (°N)	Long. (°E)						strike	dip	rake	
1	1 Mar 2008	07:01	37.897	26.811	14	10	4.4	4.1	21	309	55	–64	RMT
2	5 Feb 2009	20:08	37.911	27.110	11		3.6			117	52	–68	FMP
3	20 Jun 2009	08:28	37.660	26.869	5	4	5.1	4.9	267	115	34	–66	RMT
4	6 Sep 2009	18:36	37.719	26.811	7		3.7			152	53	–33	FMP
5	12 Sep 2009	00:50	37.537	27.015	9		4.4			285	65	–90	FMP
6	4 Aug 2010	20:38	37.488	26.984	10	16	4.0	3.7	4.24	309	58	–49	RMT
7	11 Aug 2010	02:16	37.890	26.822	9	16	3.8	3.7	4.08	31	73	–158	RMT
8	11 Oct 2010	18:03	37.908	27.311	6	6	3.6	3.3	1.09	32	47	–149	RMT
9	11 Nov 2010	19:15	37.859	27.353	6	4	3.8	3.7	4.29	277	75	–88	RMT
10	11 Nov 2010	20:08	37.860	27.370	4	6	5.0	4.7	128	256	56	–112	RMT
11	14 Nov 2010	05:21	37.870	27.344	6	6	4.2	4.1	19.2	278	64	–94	RMT
12	8 Dec 2010	21:50	37.879	27.366	8	6	4.0	3.9	7.53	266	34	–102	RMT
13	4 Feb 2011	23:12	37.894	27.317	7		3.8			110	26	–80	FMP
14	5 Feb 2011	02:37	37.881	27.305	7	6	4.0	3.9	8.52	147	24	–40	RMT
15	6 Feb 2011	02:08	37.887	27.283	8		4.2			140	16	–60	FMP
16	22 Feb 2011	15:23	37.885	27.284	7	6	3.7	3.5	2.04	107	61	–67	RMT
17	27 Dec 2011	05:59	37.966	27.186	12	8	4.3	4.0	14.4	300	54	–59	RMT
18	27 Dec 2011	07:51	37.965	27.186	9	6	4.3	4.0	11.5	300	55	–56	RMT
19	27 Jan 2012	17:43	37.490	27.120	6		4.4			292	42	–87	FMP
20[a]	3 Mar 2008	cluster	37.730	26.950	12					291	45	–60	FMP
21[b]	18 May 2012	cluster	37.790	26.750	9					274	35	–74	FMP
22[c]	31 Jul 2012	cluster	37.870	26.690	13					121	78	–21	FMP

Notes: Locations are determined in this study with the use of hypoDD program whereas fault plane solutions are determined either from first polarities (FMP) or moment tensor (RMT) inversion (solutions with estimated moment); h – focal depth, H – centroid depth.

[a)]cluster of 5 events in a radius of 1.0 km, $2.3 < M_L < 3.3$,

[b)]cluster of 9 events in a radius of 1.5 km, $2.7 < M_L < 4.3$,

[c)]cluster of 14 events in a radius of 1.5 km, $1.7 < M_L < 3.7$.

fault plane solutions determinations for the clusters in Samos Island, led us to the determination of joint fault plane solutions (20, 21, and 22 in Table 3) by using *P*-wave polarity data from the recordings of at least 5 events. The joint solutions were performed using all available polarities of the micro-seisms for achieving a composite fault plane solution for each cluster. The

network geometry secured good azimuthal coverage, providing the ability of well-constrained focal mechanisms. The *P*-wave onsets were determined for all the located events for the fault plane solutions; nevertheless, polarities errors were not allowed in the solutions. Multiple acceptable solutions exhibiting different faulting type for the same event, as well as solutions with more than ±10° uncertainties in faulting parameters determination are not taken into account in this study. For the larger events, RMT solutions were determined, using at least four stations with 3-component recordings filtered by a band-pass filter (0.03-0.1 Hz) inverted for well-constrained solutions to be obtained. Solutions from both methods, when available, are presented in a series of figures in Appendix B (Figs. B1-B13). In the case of unreliable solution derived from waveform inversion, the FMP solution is preferred (*i.e.*, event No. 5 with $M_L = 4.4$). It also happens that FMP solutions were not acceptable for some of the larger events, due to the inadequate *P*-onsets distribution (*i.e.*, event No. 6, Fig. B3).

Figure 6, where these focal mechanisms are plotted, shows a rather limited diversity of faulting style, competing between strike-slip and normal

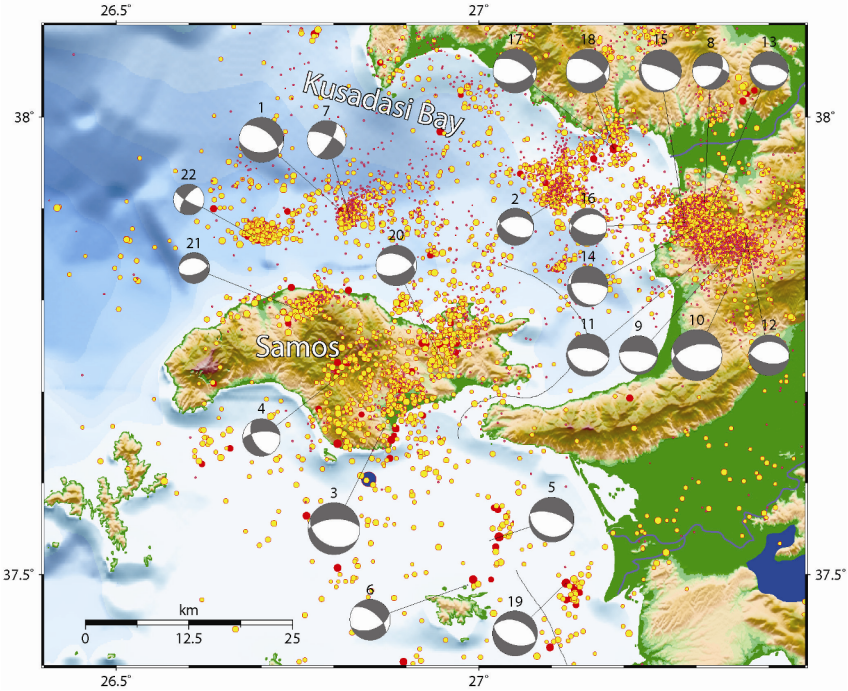

Fig. 6. Spatial distribution of local seismicity in the study area, along with fault plane solutions determined in the present study, which are shown as lower hemisphere equal area projections. Colour version of this figure is available in electronic edition only.

faulting, with most of them exhibiting an oblique motion. It is evident that the strike slip nature of the sources is more dominant in the Aegean part of our study area, whereas normal faulting is more prevalent in Kusadasi area. In all solutions the predominance of the almost N-S direction of the minimum principal stress component, *T*-axis, is obvious. In the very dense cluster and almost ESE-WNW trend of seismicity in Kusadasi area, normal faulting is more prominent on east-west striking nodal planes. Fault plane solutions were determined for nine earthquakes of this cluster, with four of them evidencing pure extension whereas the rest five exhibit oblique motion. Oblique faulting, in particular, is associated with the stronger event of this cluster, which occurred on 11 November 2010, with $M_L = 5.0$ (event No. 10 in Fig. 6). Onshore and offshore Samos Island strike-slip motion is more prevalent, and faulting type is ranging between strike slip (events Nos. 22 and 7, offshore in Fig. 6) to transtensional and even to normal faulting.

5. THE SAMOS 2009 SWARM AND DISTINCTIVE CLUSTERS

Field geology based studies revealed the location and geometry of major faults (traced with lines in Fig. 7 from Mountrakis *et al.* 2003), considered to be responsible for the strong historical events presented in the previous section. We recall as the most recent and significant earthquake, the 1904 $M = 6.8$ event, which caused severe damage to the towns and villages along the northwestern coastal area. Despite the criticalness of such occurrences, we still ignore the geometry at depth of the causative faults. Station coverage from the Hellenic National Seismological Network is not adequate to provide such quality and quantity of data as to detect and analyze microseismicity along this active fault system, which is now provided from the local network.

The 2009 Samos swarm consists the most intense activity during the operation of the network started near the town of Phythagorion, southeastern Samos, on 20 June, with an event of $M_w = 5.1$ with more than 80 events with $M_L > 1.5$ in the first 10 days (Fig. 7). The largest earthquake was widely felt in Samos and the neighbor islands, as well as across the coastal area of western Turkey. The causative fault of this activity, which is rather sparse, than aligned to form a stripe of epicenters, was sought among the known mapped faults (PF in Fig. 7, Mountrakis *et al.* 2003). A second cluster was observed close to the northeastern coast of the Island, where a longer fault segment is mapped, namely the Kokkari-Vathi fault (KVF in Fig. 7, again by Mountrakis *et al*. 2003), which runs parallel to the previously mentioned one. Therefore, a cross section is constructed normal to the strike of both these faults segments, based on the events comprised in the AA′ box, and shown in the lower part of Fig. 7. It is evidenced that the two segments are aligned parallel also in depth, dipping to the south and being active up to

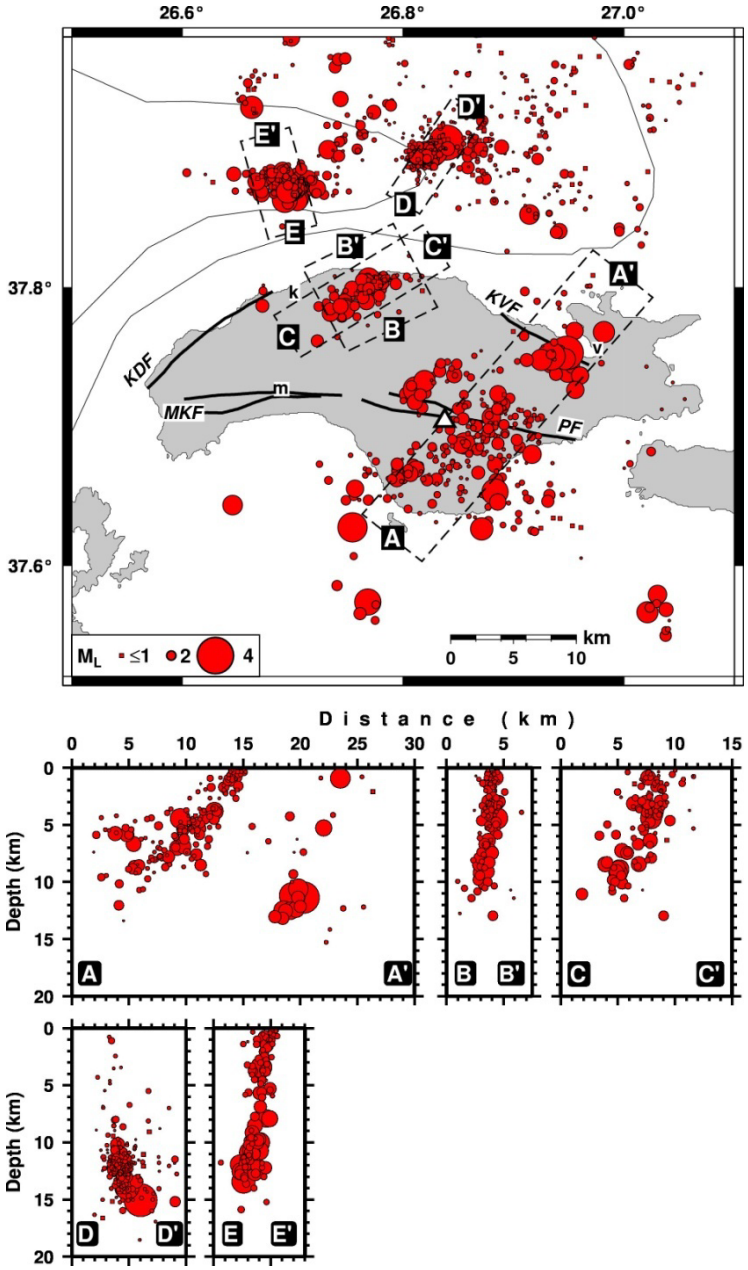

Fig. 7. Map view and the vertical cross sections of seismicity in five clusters onshore and offshore Samos Island. k – Karlovasi, m – Marathokampos, v – Vathi, KDF – Karlovassi-Drakei Fault, KVF – Kokkari-Vathi Fault, MKF – Marathokampos-Kerketeas Fault, PF – Pythagorion Fault.

12 km, where the focus of the strong $M_w = 5.1$ event is also located. It could be inferred, alike in most normal faults, that at depth the average dip is lower, while towards the surface it becomes steeper. The verification of south dipping normal faults onto the Island of Samos is a major finding of this work, since it is the first time that seismological data were available to reveal the properties of these active structures.

The cluster located near the central northern coastal part of the Island cannot be directly associated with any of the known mapped faults and seems to reveal a secondary segment, adjacent to Karlovassi–Drakei fault. Although it is aligned in a NE-SW direction, a strike normal cross section (BB′) shows an almost vertical fault, whereas the strike parallel cross section (CC′) rather reveals a south-dipping fault, compatible with the previous two activated segments (KVF and PF). This means that its longer dimension on a map view does not represent the along-strike epicentral alignment, but the surface projection of the along-dip direction epicentral position.

Two more clusters are identified offshore, comprising an adequate number of events each one, capable for the identification of a slightly north dipping fault from the first one (DD′ cross section), compatible with the north dipping nodal planes of fault plane solutions numbered 1 and 7 in Table 3 and Fig. 6, and an almost vertical with a slight dip to the south for the second one (EE′ cluster and cross section) again compatible with the south dipping nodal plane of the fault plane solution numbered 22 in Table 3 and Fig. 6.

6. GEOMETRY OF THE KUSADASI NORMAL FAULT SYSTEM

The cluster located near Kusadasi is the most dense one in our data sample and located in the fault-bounded Kusadasi basin, meaning that seismicity may be the manifestation of activity on both north-dipping and south-dipping faults, traced as continuous lines in the map of the upper part of Fig. 8. The Kusadasi fault is considered as a young and prominent fault zone, which extends toward Aegean, a typical oblique with right lateral and normal displacements (Gurer *et al.* 2001). Vertical cross sections AA′ and BB′ taken to be perpendicular to the fault strike, do not show any preference for the fault dip direction, but rather display vertical fault with seismicity distributed from the surface up to a depth of 20 km. The details revealed for this fault system from the DD relocations are compared with the available fault plane solutions (Fig. 6). Although not identical, the solutions support a north dipping steep nodal plane which is in agreement with the mapped Kusadasi fault.

Smaller offshore clusters can be seen also, and the ones with an adequate number of earthquakes are taken into consideration. The vertical cross-section CC′ comprises three distinctive clusters aligned in parallel with a predominant NW-SE strike, in accordance with the slightly south dipping

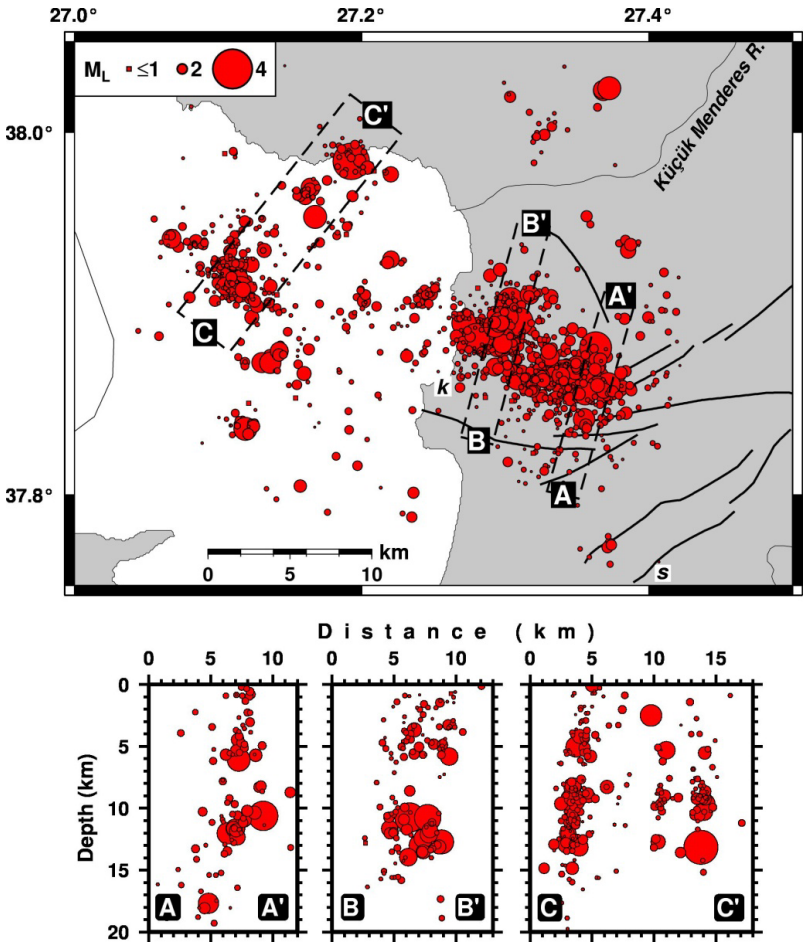

Fig. 8. Map view and the vertical cross sections of seismicity in Kusadasi area. k – Kusadasi, s – Soke.

nodal plane of the solutions numbered 17 and 18 in Fig. 6, for the northernmost cluster and the solution numbered 2 for the southernmost segment. The transtensional nature of the motion is also evidenced here, an important observation for signifying the boundaries between this and strike-slip movement, evidenced in the 1992 and 2005 sequences (Aktar *et al.* 2007, Benetatos *et al.* 2006) that were located just to the west adjacent fault segments.

7. DISCUSSION

Eastern Aegean constitutes a complex tectonic transitional area that is influenced by the back arc opening and strike slip motion translated from the motion taking place along the North Anatolian Fault and its continuation in

Northern Aegean Sea. The contribution of the present study is the identification of the seismotectonic properties of the study area, as detailed as possible, through the exploitation, for a first time, of microseismicity as it derived from the recordings of a dense local network. This resulted in highly accurate locations and low magnitude threshold, with the microearthquake alignments being used in turn to unravel at depth the detailed geometry of the fault systems. This is a prerequisite for investigating seismic activity and retrieving source parameters around recognized active faults.

Most of the relocated earthquakes are clustered, as it usually happens with microseismicity following a cascade type behavior, and bringing in the foreground some of the activated structures thus providing precious information for their properties, and leaving other unvisited, in particular when the operation of the local seismological network is limited in time. The major faults of the study area were never associated with coseismic observations recently, for a correspondence between active faults and earthquakes to be established. Therefore, the knowledge of their properties is fundamental for evaluating the deformation style and consequently the seismic hazard.

Fault plane solutions exhibit slight differentiations in the faulting style in some places, in particular in Kusadasi area, possibly associated with local variations of the seismogenic conditions due to mechanical heterogeneities. The significant contribution of the study is the detailing of the local active structures and their properties, identified by the microseismicity, to forecasting future locations of strong earthquakes. The hypothesis that underlies this approach is that the smaller earthquakes are delineating locations that are capable of generating larger earthquakes.

8. CONCLUSIONS

Accurately located microseismicity that took place in the eastern and central Aegean area, contributed to the association of specific earthquake clusters with mapped faults inland. This association shed more light in faulting properties recognition for the major structures that constitute important components for seismic hazard evaluation. For the Samos fault system, in particular, which is responsible for the strongest known catastrophic earthquakes in the study area, the most recent one being the 1904 (M6.8) event, identification of geometry and kinematics became feasible.

The determined focal mechanisms enabled the recognition of stress pattern in the study area. Fault plane solutions evaluated from both P-wave polarity data and moment tensor analysis, show the predominance of normal faulting, along with strong contribution of the strike slip motion, with a N-S trending direction of extension, coherent with the regional stress field in the Aegean area. The transtensional faulting mechanisms are characteristic for the transition zone of deformation between the Anatolian and Aegean

microplates, signifying probably the transition from pure strike slip faulting along the North Anatolian and its continuation to the west, North Aegean Trough, and the back arc extension of the southern Aegean. The mapped known faults onshore Samos Island were partly activated in very limited patches, and therefore may be presently considered locked.

Acknowledgments. This work was partially supported by the research project "Seismotectonic properties of the eastern Aegean: Implications on the stress field evolution and seismic hazard assessment in a tectonically complex area", GSRT 10 TUR/1-3-9, Joint Research and Technology Programmes 2010-2011, financed by the Ministry of Education of Greece and the Scientific and Technological Research Council of Turkey (TUBITAK 109Y401). Valuable comments from Marc-André Lambert and an anonymous reviewer are greatly appreciated. Gratitude is also extended to the editorial assistance of Beatriz Quintal. The GMT program (Wessel and Smith 1998) was used for plotting the figures. Geophysics Department Contribution 818.

Appendix A

Focal mechanisms from *P*-wave first motion polarities

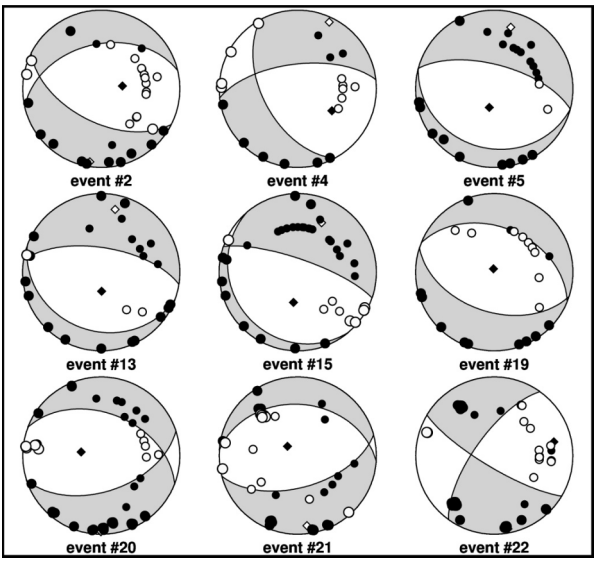

Fig. A1. *P*-wave first motion polarities of the 4 events and 3 clusters. The event numbers are given beneath the focal spheres (see Table 3). The compressional quadrants are shaded in gray. The black and white circles refer to up and down *P*-wave first motion polarities, respectively. P and T axes are also represented by the solid and open diamonds, respectively.

Appendix B

Focal mechanisms determined with RMT inversion

The fault plane solutions of the 13 events were determined with the RMT inversion. Only the seismograms that were recorded by stations located between 30 and 200 km were used for the solutions implemented with the ISOLA local moment tensor inversion algorithm (Sokos and Zahradnik 2008). At least four stations and three components waveforms filtered between the frequency bands of 0.03-0.1 Hz were inverted for events. The minimum misfit solutions of the earthquakes are shown in Figs. B1-B13. The black and grey lines are un-normalised observed and synthetic waveforms, respectively. The station code is shown to the left of three component waveforms (NS, EW, and Z). The percentages of variance reduction (VR) and double couple component (DC) are given below the MT focal mechanism solution. Some of the events have also *P*-wave first motion polarity solutions (FMP). These solutions are given with *P*-wave first motion polarities (black and white circles are up and down motion, respectively) on lower hemisphere projection.

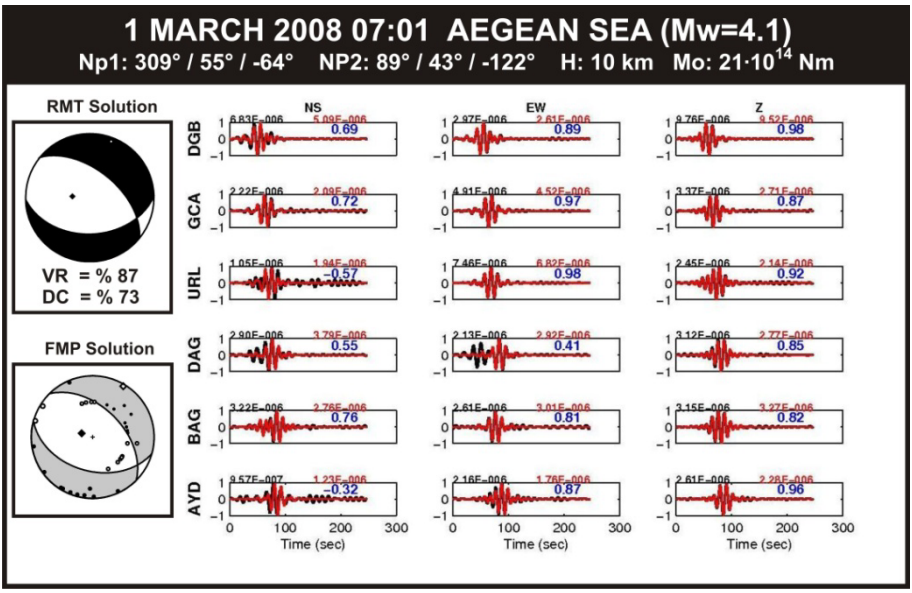

Fig. B1. The RMT inversion solution of the 1 March 2008, 07:01 earthquake.

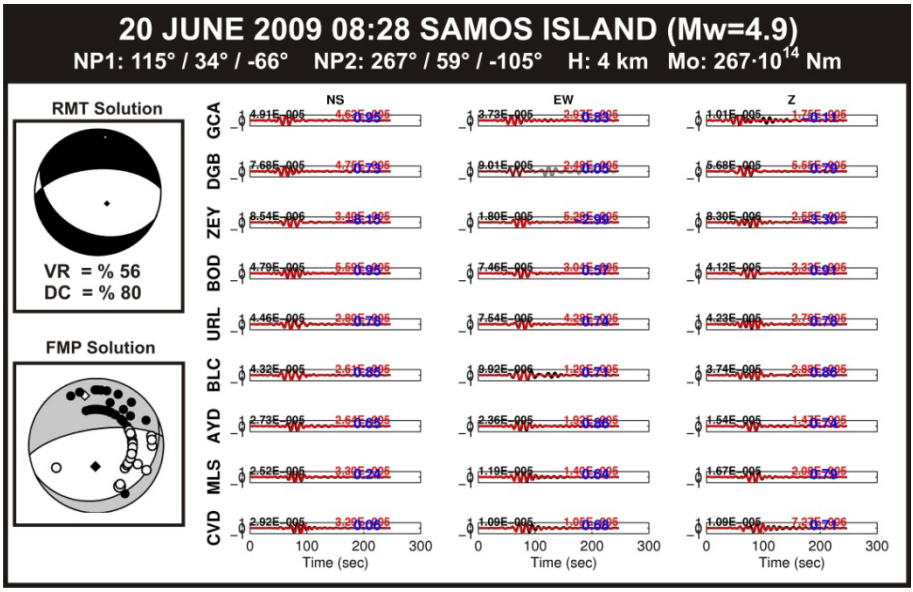

Fig. B2. The RMT inversion solution of the 20 June 2009, 08:28 earthquake.

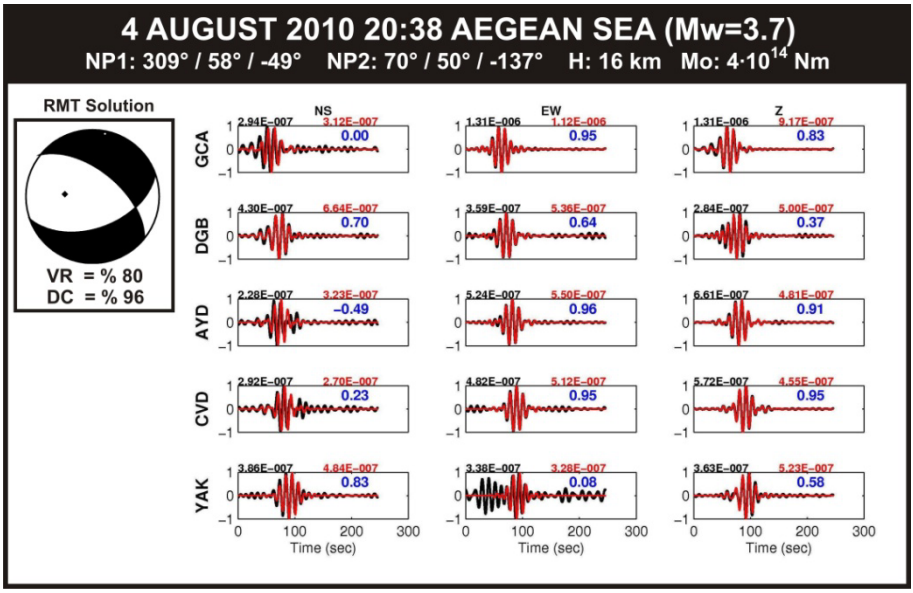

Fig. B3. The RMT inversion solution of the 4 August 2010, 20:38 earthquake.

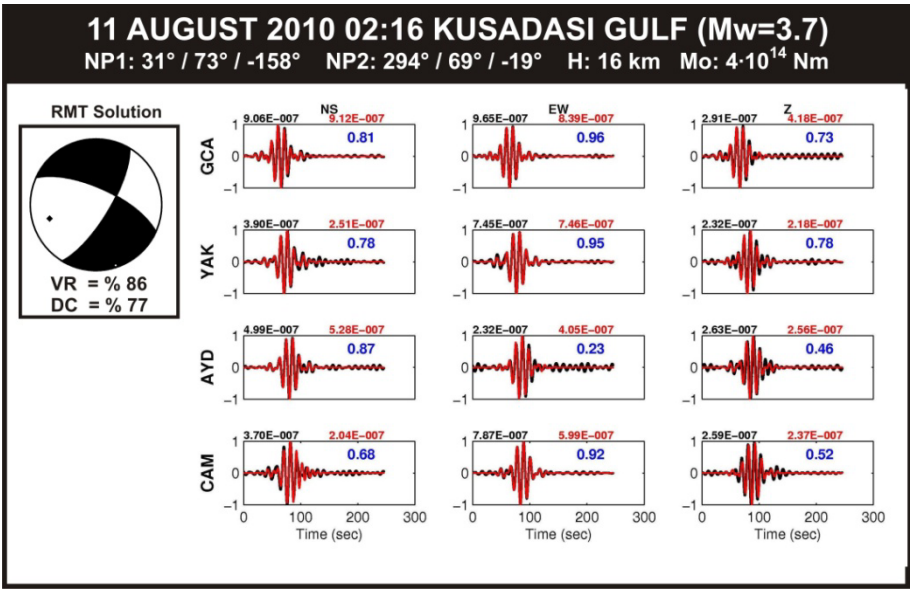

Fig. B4. The RMT inversion solution of the 11 August 2010, 02:16 earthquake.

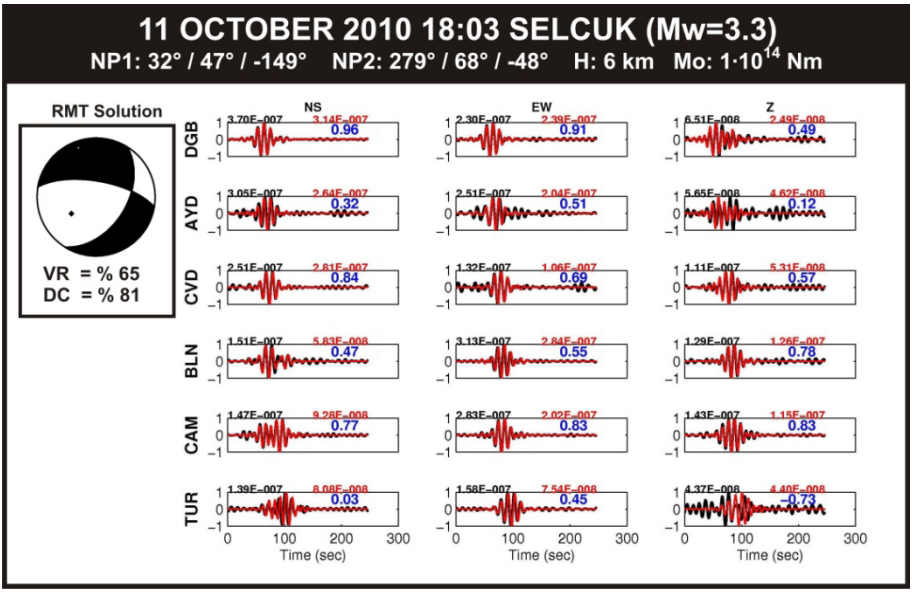

Fig. B5. The RMT inversion solution of the 11 October 2010, 18:03 earthquake.

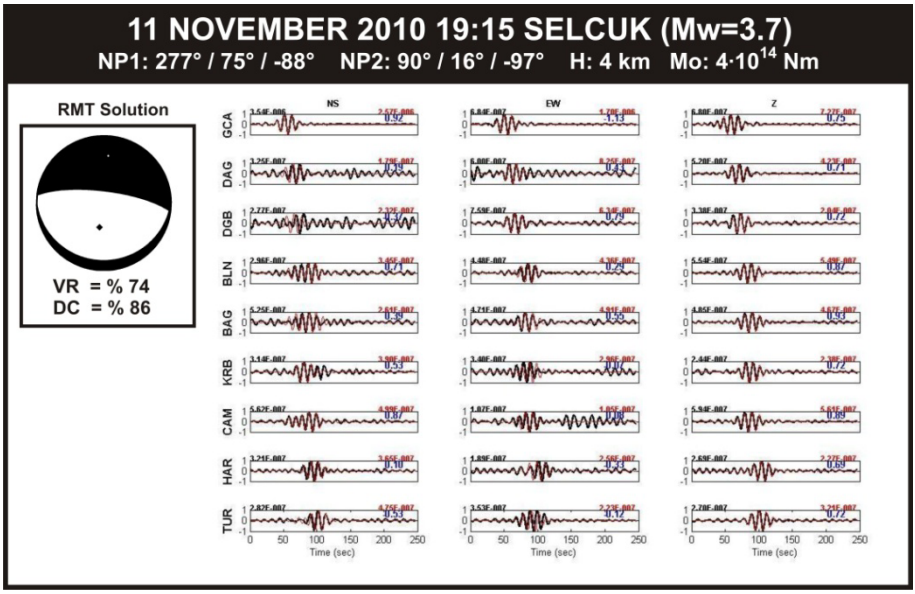

Fig. B6. The RMT inversion solution of the 11 November 2010, 19:15 earthquake.

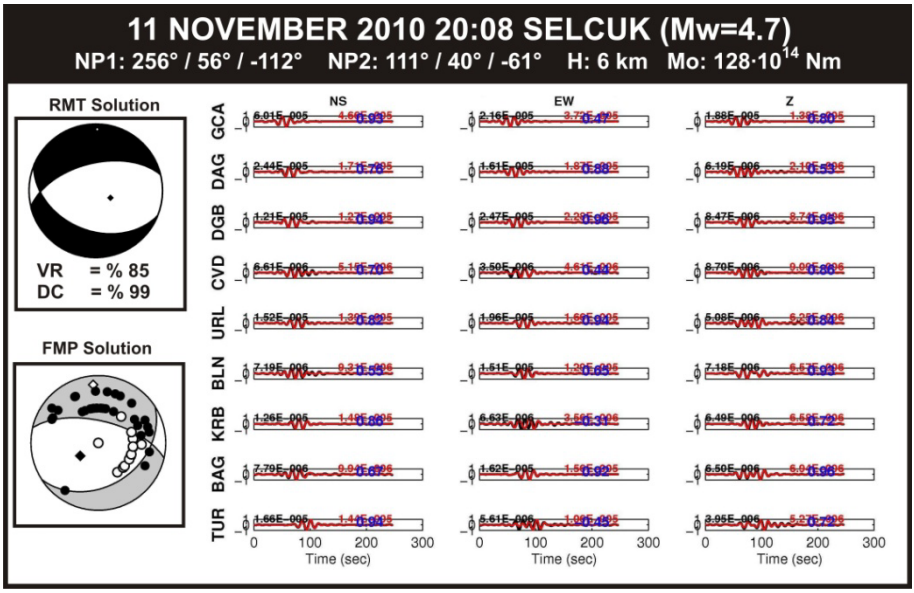

Fig. B7. The RMT inversion solution of the 11 November 2010, 20:08 earthquake.

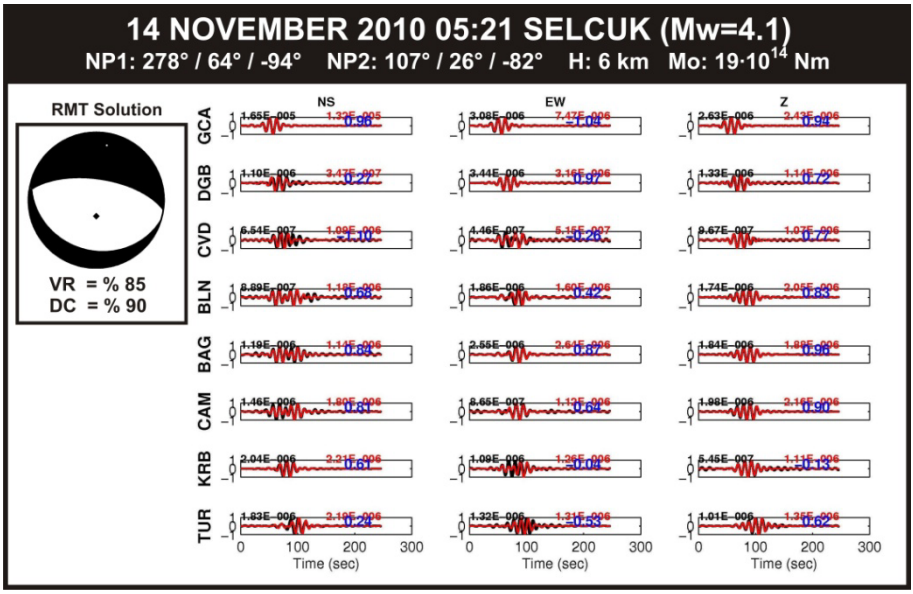

Fig. B8. The RMT inversion solution of the 14 November 2010, 05:21 earthquake.

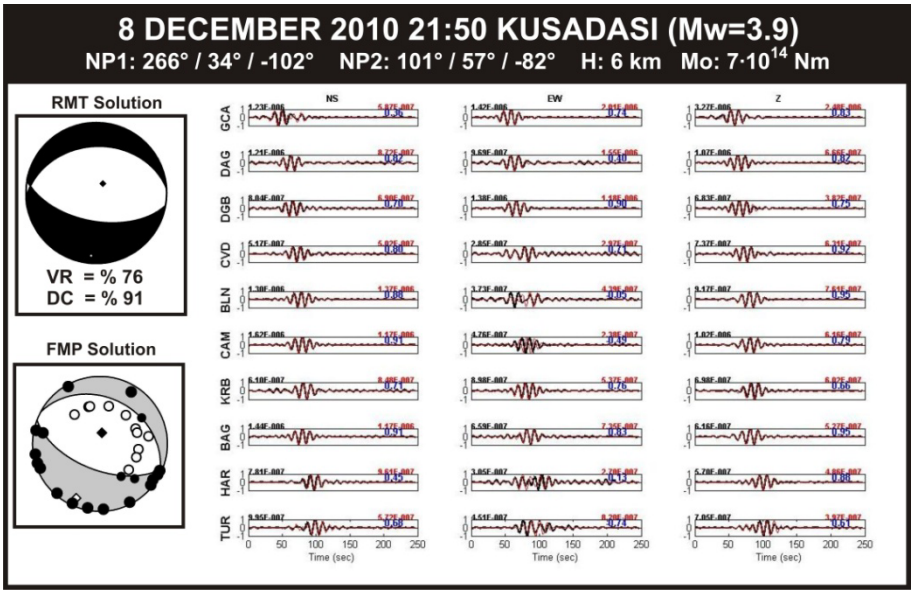

Fig. B9. The RMT inversion solution of the 8 December 2010, 21:50 earthquake.

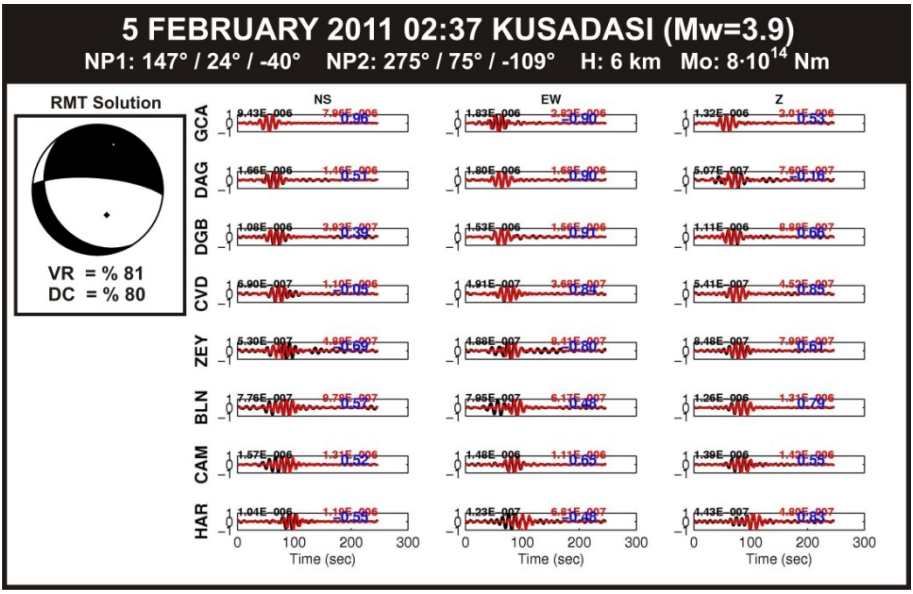

Fig. B10. The RMT inversion solution of the 5 February 2011, 02:37 earthquake.

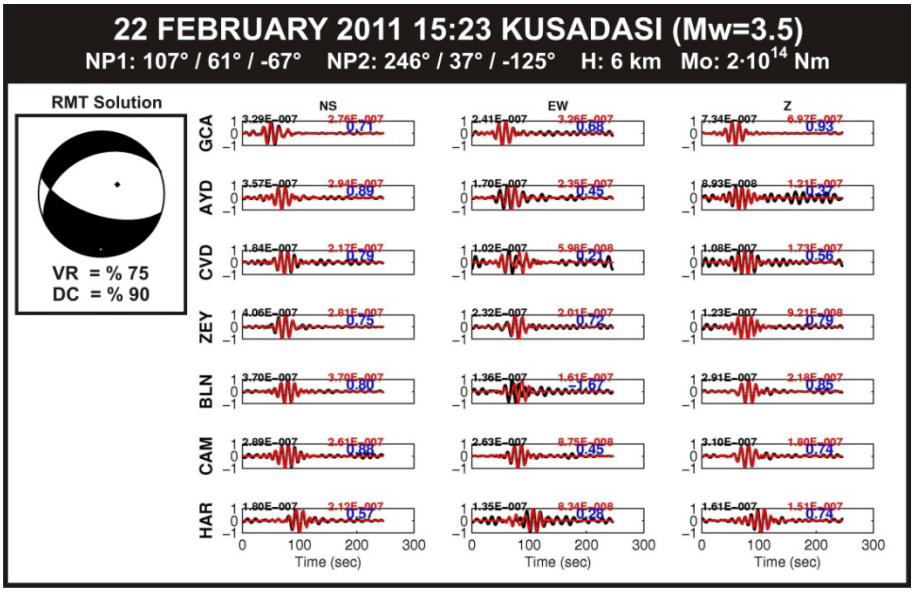

Fig. B11. The RMT inversion solution of the 22 February 2011, 15:23 earthquake.

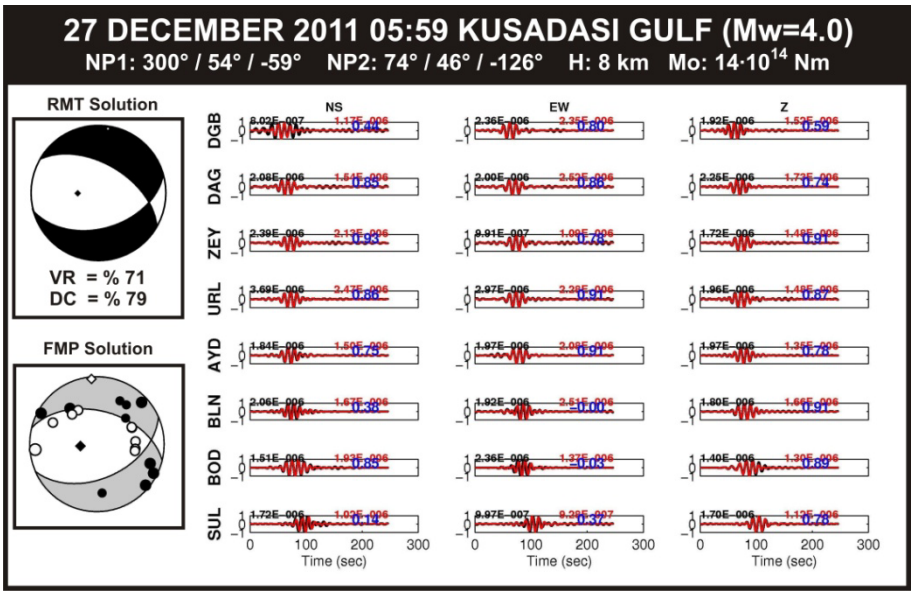

Fig. B12. The RMT inversion solution of the 27 December 2011, 05:59 earthquake.

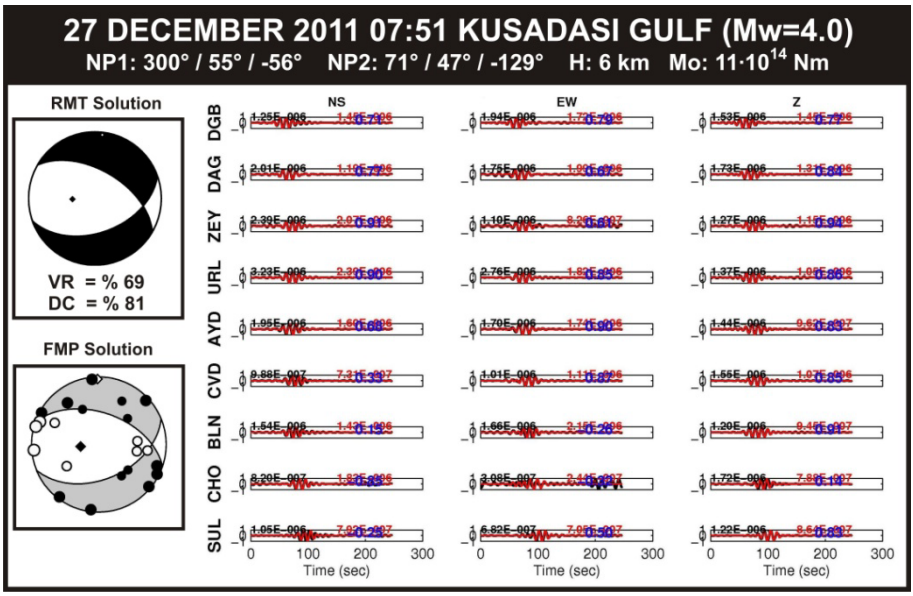

Fig. B13. The RMT inversion solution of the 27 December 2011, 07:51 earthquake.

References

Aktar, M., H. Karabulut, S. Özalaybey, and D. Childs (2007), A conjugate strike-slip fault system within the extensional tectonics of Western Turkey, *Geophys. J. Int.* **171**, 3, 1363-1375, DOI: 10.1111/j.1365-246X.2007.03598.x.

Aktug, B., J.M. Nocquet, A. Cingöz, B. Parsons, Y. Erkan, P. England, O. Lenk, M.A. Gürdal, A. Kilicoglu, H. Akdeniz, and A. Tekgül (2009), Deformation of western Turkey from a combination of permanent and campaign GPS data: Limits to block-like behavior, *J. Geophys. Res.* **114**, B10, DOI: 10.1029/2008JB006000.

Akyol, N., L. Zhu, B.J. Mitchell, H. Sözbilir, and K. Kekovalı (2006), Crustal structure and local seismicity in western Anatolia, *Geophys. J. Int*. **166**, 3, 1259-1269, DOI: 10.1111/j.1365-246X.2006.03053.x.

Benetatos, C., A. Kiratzi, A. Ganas, M. Ziazia, A. Plessa, and G. Drakatos (2006), Strike-slip motions in the Gulf of Siğaçik (western Turkey): Properties of the 17 October 2005 earthquake seismic sequence, *Tectonophysics* **426**, 3-4, 263-279, DOI: 10.1016/j.tecto.2006.08.003.

Bozkurt, E. (2001), Neotectonics of Turkey – a synthesis, *Geodin. Acta* **14**, 1-3, 3-30, DOI: 10.1016/S0985-3111(01)01066-X.

Bozkurt, E. (2003), Origin of NE-trending basins in western Turkey, *Geodin. Acta* **16**, 2-6, 61-81, DOI: 10.1016/S0985-3111(03)00002-0.

Çiftçi, N.B., and E. Bozkurt (2009), Pattern of normal faulting in the Gediz Graben, SW Turkey, *Tectonophysics* **473**, 1-2, 234-260, DOI: 10.1016/ j.tecto.2008. 05.036.

Genç, C.Ş., Ş. Altunkaynak, Z. Karacık, M. Yazman, and Y. Yılmaz (2001), The Çubukludağ graben, south of İzmir: its tectonic significance in the Neogene geological evolution of the western Anatolia, *Geodin. Acta* **14**, 1-3, 45-55, DOI: 10.1016/S0985-3111(00)01061-5.

Gürer, Ö.F., M. Bozcu, K. Yilmaz, and Y. Yilmaz (2001), Neogene basin development around Söke-Kuşadası (western Anatolia) and its bearing on tectonic development of the Aegean region, *Geodin. Acta* **14**, 1-3, 57-69, DOI: 10.1016/S0985-3111(00)01059-7.

Inan, S., S. Ergintav, R. Saatçilar, B. Tüzel, and Y. İravul (2007), Turkey makes major investment in earthquake research, *EOS Trans. Am. Geophys. Union* **88**, 34, 333-334, DOI: 10.1029/2007EO340002.

Karakostas, V.G., E.E. Papadimitriou, G.F. Karakaisis, C.B. Papazachos, E.M. Scordilis, G. Vargemezis, and E. Aidona (2003), The 2001 Skyros, Northern Aegean, Greece, earthquake sequence: off-fault aftershocks, tectonic implications, and seismicity triggering, *Geophys. Res. Lett.* **30**, 1, 12-1-12-4, DOI: 10.1029/2002GL015814.

Kurt, H., E. Demirbağ, and İ. Kuşçu (1999), Investigation of the submarine active tectonism in the Gulf of Gökova, southwest Anatolia – southeast Aegean

Sea, by multi-channel seismic reflection data, *Tectonophysics* **305**, 4, 477-496, DOI: 10.1016/S0040-1951(99)00037-2.

Lienert, B.R., and J. Havskov (1995), A computer program for locating earthquakes both locally and globally, *Seismol. Res. Lett.* **66**, 5, 26-36, DOI: 10.1785/gssrl.66.5.26.

McClusky, S., S. Balassanian, A. Barka, C. Demir, S. Ergintav, I. Georgiev, O. Gurkan, M. Hamburger, K. Hurst, H. Kahle, K. Kastens, G. Kekelidze, R. King, V. Kotzev, O. Lenk, S. Mahmoud, A. Mishin, M. Nadariya, A. Ouzounis, D. Paradisis, Y. Peter, M. Prilepin, R. Reilinger, I. Sanli, H. Seeger, A. Tealeb, M.N. Toksöz, and G. Veis (2000), Global Positioning System constraints on plate kinematics and dynamics in the eastern Mediterranean and Caucasus, *J. Geophys. Res.* **105**, B3, 5695-5719, DOI: 10.1029/1999JB900351.

McKenzie, D. (1972), Active tectonics of the Mediterranean region, *Geophys. J. Roy. Astr. Soc.* **30**, 2,109-185, DOI: 10.1111/j.1365-246X.1972.tb02351.x.

McKenzie, D. (1978), Active tectonics of the Alpine–Himalayan belt: the Aegean Sea and surrounding regions, *Geophys. J. Roy. Astr. Soc.* **55**, 1, 217-254, DOI: 10.1111/j.1365-246X.1978.tb04759.x.

Mountrakis, D., A. Kilias, E. Vavliakis, A. Psilovikos, and E. Thomaidou (2003) Neotectonic map of Samos Island (Aegean Sea, Greece): Implication of Geographical Information Systems in the geological mapping. **In:** *4th European Congress on Regional Geoscientific Cartography and Information Systems, Bologna, Italy*, 11-13.

Nocquet, J.-M. (2012), Present-day kinematics of the Mediterranean: A comprehensive overview of GPS results, *Tectonophysics* **579**, 220-242, DOI: 10.1016/j.tecto.2012.03.037.

Ocakoğlu, N., E. Demirbag, and İ. Kuşçu (2004), Neotectonic structures in the area offshore of Alaçati, Doğanbey and Kuşadası (western Turkey): evidence of strike-slip faulting in the Aegean extensional province, *Tectonophysics* **391**, 1-4, 67-83, DOI: 10.1016/j.tecto.2004.07.008.

Papazachos, B.C., and P.E. Comninakis (1971), Geophysical and tectonic features of the Aegean Arc, *J. Geophys. Res.* **76**, 35, 8517-8533, DOI: 10.1029/JB076i035p08517.

Papazachos, B.C., E.E. Papadimitriou, A.A. Kiratzi, C.B. Papazachos, and E.K. Louvari (1998), Fault plane solutions in the Aegean Sea and the surrounding area and their tectonic implication, *Boll. Geof. Teor. Appl.* **39**, 3, 199-218.

Papazachos, C.B. (1999), Seismological and GPS evidence for the Aegean–Anatolia interaction, *Geophys. Res. Lett.* **26**, 17, 2653-2656, DOI: 10.1029/1999GL900411.

Snoke, J.A., J.W. Munsey, A.G. Teague, and G.A. Bollinger (1984), A program for focal mechanism determination by combined use of polarity and SV-P amplitude ratio data, *Earthq. Notes* **55**, 3, 15.

Sokos, E.N., and J. Zahradnik (2008), ISOLA a Fortran code and a Matlab GUI to perform multiple-point source inversion of seismic data, *Comput. Geosci.* **34**, 8, 967-977, DOI: 10.1016/j.cageo.2007.07.005.

Tan, O. (2013), The dense micro-earthquake activity at the boundary between the Anatolian and South Aegean microplates, *J. Geodyn.* **65**, 199-217, DOI: 10.1016/j.jog.2012.05.005.

Tan, O., M.C. Tapırdamaz, S. Ergintav, S. İnan, Y. İravul, R. Saatçilar, B. Tüzel, A. Tarancioğlu, S. Karakisa, R.F. Kartal, S. Zünbül, K. Yanik, M. Kaplan, F. Şaroğlu, A. Koçyiğit, E. Altunel, and N.M. Özel (2010), Bala (Ankara) earthquakes: Implications for shallow crustal deformation in Central Anatolian section of the Anatolian platelet (Turkey), *Turkish J. Earth Sci.* **19**, 4, 449-471, DOI: 10.3906/yer-0907-1.

Taymaz, T., J. Jackson, and D. McKenzie (1991), Active tectonics of the north and central Aegean Sea, *Geophys. J. Int*. **106**, 2, 433-490, DOI: 10.1111/j.1365-246X.1991.tb03906.x.

Waldhauser, F., and W.L. Ellsworth (2000), A double-difference earthquake location algorithm: method and application to the northern Hayward fault, California, *Bull. Seismol. Soc. Am*. **90**, 6, 1353-1368, DOI: 10.1785/0120000006.

Wessel, P., and W.H.F. Smith (1998), New, improved version of the Generic Mapping Tools released, *EOS Trans. Am. Geophys. Union* **79**, 47, 579, DOI: 10.1029/98EO00426.

Received 2 May 2013
Received in revised form 3 October 2013
Accepted 21 October 2013